Original Article

Renal ischemia-reperfusion injury in rabbits evaluated with quantitative susceptibility mapping: an animal study

Kai Luo[1#], Anding Yu[1#], Qinglin Fu[1], Liang Pan[1], Weiqiang Dou[2], Jinggang Zhang[1], Jie Chen[1]

[1]Department of Radiology, The Third Affiliated Hospital of Soochow University, Changzhou, China; [2]MR Research China, GE Healthcare, Beijing, China

Contributions: (I) Conception and design: K Luo, J Zhang, J Chen; (II) Administrative support: J Zhang, J Chen; (III) Provision of study materials or patients: K Luo, A Yu, J Zhang, J Chen; (IV) Collection and assembly of data: K Luo, A Yu, Q Fu; (V) Data analysis and interpretation: K Luo, L Pan, W Dou, J Zhang; (VI) Manuscript writing: All authors; (VII) Final approval of manuscript: All authors.

[#]These authors contributed equally to this work.

Correspondence to: Jinggang Zhang; Jie Chen. Department of Radiology, The Third Affiliated Hospital of Soochow University, 185 Juqian Street, Changzhou 213003, China. Email: yanqing84@126.com; slqyuer@126.com.

Background: There were no effective noninvasive methods to diagnose renal ischemia-reperfusion injury (IRI), which is a major clinical problem. The objective of this study was to explore the feasibility of the quantitative susceptibility mapping (QSM) technique in evaluating the dynamic changes in the renal IRI process.

Methods: A total of 36 New Zealand rabbits were randomly assigned to the IRI group (n=30) and the sham group (n=6). All rabbits underwent magnetic resonance imaging (MRI) examination, including T2-weighted imaging and QSM before the operation (pre-IRI) and 1, 12, 24, and 48 h after the operation (IRI-1h, IRI-12h, IRI-24h, and IRI-48h, respectively). Regions of interest were manually delineated in the outer medulla. All specimens were stained with hematoxylin and eosin (HE) and glutathione peroxidase 4 (GPX4). The pathological score of renal injury and the average optical density value of GPX4 were calculated. The repeated measurement analysis of variance (ANOVA) and Spearman correlation analysis were used to compare the differences between the susceptibility values and determine the correlation.

Results: In the IRI group, the susceptibility values of the outer medulla at the pre-IRI, IRI-1h, IRI-12h, IRI-24h, and IRI-48h time points were $(42.83\pm7.83)\times10^{-3}$, $(-5.33\pm6.28)\times10^{-3}$, $(6.50\pm3.94)\times10^{-3}$, $(12.00\pm3.74)\times10^{-3}$, and $(22.00\pm6.81)\times10^{-3}$ ppm, respectively. The susceptibility values significantly differed among the different time points ($P<0.001$). The susceptibility values had a negative correlation with the scores of cell edema ($\rho=-0.61$; $P=0.002$) and the average optical density value of GPX4 ($\rho=-0.70$; $P<0.001$). The susceptibility values had a positive correlation with iron content ($\rho=0.79$; $P<0.001$), the scores of cell necrosis ($\rho=0.71$; $P<0.001$), interstitial inflammation ($\rho=0.60$; $P=0.002$), cast ($\rho=0.75$; $P<0.001$), and the total pathological score of renal injury ($\rho=0.51$; $P=0.01$).

Conclusions: QSM can be used as a noninvasive method to assess the dynamic changes of the outer medulla in the early stage of renal IRI in rabbits.

Keywords: Ischemia-reperfusion injury (IRI); quantitative susceptibility mapping (QSM); kidney; magnetic resonance imaging (MRI)

Submitted Aug 10, 2022. Accepted for publication Feb 11, 2023. Published online Mar 03, 2023.
doi: 10.21037/qims-22-838
View this article at: https://dx.doi.org/10.21037/qims-22-838

Introduction

Renal ischemia-reperfusion injury (IRI) can occur in the process of cardiovascular surgery, renal transplantation, shock, and severe trauma, and it is one of the main causes of acute kidney injury (AKI) and delayed recovery of transplanted kidney (1). Therefore, diagnosing and monitoring renal IRI in the early stage is essential.

Currently, the clinical diagnosis of IRI is based on biochemical and hematologic tests. However, biochemical markers, such as serum creatinine and urinary microprotein, have a lagging effect and cannot be used to evaluate the function of a single kidney. Renal puncture biopsy is the gold standard for evaluating renal injury, but its clinical application is limited because of its invasiveness, ease of infection, and other complications (2).

Functional magnetic resonance imaging (MRI), including diffusion-weighted imaging (DWI), blood oxygen level-dependent magnetic resonance imaging (BOLD-MRI), arterial spin labeling (ASL), and dynamic contrast-enhanced magnetic resonance imaging (DCE-MRI), has achieved satisfactory results for evaluating renal IRI. DWI uses the Brownian motion of water molecules to evaluate the structure and function of kidneys. It can provide information about the diffusion of water molecules in intracellular and extracellular space and tissue microcirculation perfusion. In their study, Hueper *et al.* (3) confirmed that the value of the apparent diffusion coefficient (ADC) decreased significantly after AKI, and the ADC value of a severe AKI group was lower than that of a moderate AKI group. However, the principle of DWI imaging is complicated. A low b value mainly reflects the perfusion factor, and an ultra-high b value ($b>2,500$ s/mm^2) mainly reflects the change of microscopic aquaporin. There are many kinds of DWI postprocessing models, and research results vary depending on the choice of model. BOLD-MRI can reflect the level of tissue oxygenation and evaluate renal IRI indirectly (4,5). However, BOLD-MRI cannot distinguish whether changes in the concentration of deoxyhemoglobin are caused by perfusion or tissue metabolism. BOLD-MRI cannot absolutely quantify the renal oxygen environment (6). ASL uses water protons as the endogenous tracer to noninvasively reflect the blood perfusion level of the kidney without the administration of a contrast agent. Hueper *et al.* (7) demonstrated that the degree of renal perfusion impairment after AKI measured using ASL imaging significantly correlated with subsequent tubular injury measured at histologic examination and kidney volume. However, due to the low signal-to-noise ratio of ASL, existing research is limited to the cortex. The reliability of the medullary perfusion value needs to be improved, but the medulla is the most typical site of renal IRI. The renal ASL sequence needs to be optimized. DCE-MRI reflects the most intuitive changes of blood flow in the cortex and medulla after renal IRI by injecting a contrast medium; however, this contrast medium can cause renal injury, so its application is limited.

Quantitative susceptibility mapping (QSM) is a new imaging technique for the quantitative analysis of tissue magnetic susceptibility. QSM has mainly been used in the central nervous system, with other related studies in the liver, kidney, heart, blood vessels, and cartilage also being conducted (8-10). Iron is paramagnetic, and the change in iron content can cause a change in tissue magnetic susceptibility. Therefore, QSM can detect a change in iron content (11). Recent studies have confirmed that ferroptosis plays an important role in the occurrence and development of renal IRI. The main manifestations of ferroptosis are iron overload and inactivation of glutathione peroxidase 4 (GPX4), which lead to the accumulation of iron-dependent lipid peroxide (12,13). Linkermann *et al.* (14) used ferrostatins to inhibit ferroptosis and demonstrated that ferrostatins could alleviate acute renal injury caused by IRI. Therefore, the purpose of this study was to explore the feasibility of using the QSM technique to evaluate the microscopic changes in iron content and the dynamic changes in the process of renal IRI. New Zealand rabbits have a larger renal volume than rats and are more suitable for evaluating MRI equipment for clinical application. Therefore, we chose New Zealand rabbits as the experimental subjects. We present the following article in accordance with the ARRIVE reporting checklist (available at https://qims.amegroups.com/article/view/10.21037/qims-22-838/rc).

Methods

Animal model

All experimental protocols were approved by the Ethics Committee of The Third Affiliated Hospital of Soochow University (No. 2020-120) and were performed according to the Guide for the Care and Use of Laboratory Animals. The sample size was calculated using the "Tests for Two Means in a Repeated Measures Design" procedure in PASS 2021 (NCSS, LLC, Kaysville, UT, USA). The power of the test was selected as 90%. In all, 36 healthy male New Zealand rabbits [the Jiangsu Science Standard Medical

Testing Co. Ltd., Changzhou, Jiangsu, China; license No. SYXK(SU)2017-0009], aged 2–3 months old and weighing 1.5–2 kg, were numbered according to a random number table. All rabbits were randomly divided into the IRI group (n=30) and the sham group (n=6). Rabbits were housed in sterile isolation cages with a temperature of 22±2 ℃ and in a 12-hour light-dark cycle. Standard chow and sterile water were available ad libitum. All rabbits were prohibited from consuming food and water 12 hours before the operation. During the operation, rabbits were anesthetized with an intramuscular injection of 3% pentobarbital sodium solution (1 mL/kg). Additionally, maintenance anesthesia was administered via the inhalation of isoflurane (2–3% isoflurane with 100% oxygen, 3 L/min) through a breathing mask. In the IRI group, the rabbits were fixed on the operating table, and the temperature of the operating table was kept at 37 ℃. The rabbits were maintained in the right decubitus position, and the 5-cm radius around the kidney was disinfected. The skin was cut with a scalpel along the longitudinal axis of the left kidney to fully expose the left renal pedicle. Forceps were used to separate the renal pedicle and ureter. Then, noninvasive vascular clips were used to cross the renal pedicle and clamp the renal pedicle. When the kidney color changed from pink to dark red, this indicated that the renal pedicle vessels were successfully clamped. The surface of the kidney was covered with wet gauze soaked in warm saline. After 60 min, the vascular clip was released. When the kidney color changed from dark red to pink, this indicated that reperfusion was successful. Finally, the kidney was reset and sutured. In the sham group, only the procedure of exposing the kidney was performed without clamping the renal pedicle. Previous studies confirmed that the renal pathophysiology significantly changes at 12 and 24 h after reperfusion, and AKI was the most severe at 48 h after reperfusion (15-17). A time point of 1 h after reperfusion was chosen to observe the changes at the beginning of reperfusion. Therefore, time points at 1, 12, 24, and 48 h after the operation were chosen to perform the MRI examination. All rabbits underwent an MRI examination before the IRI operation (pre-IRI), and 1, 12, 24, and 48 h after the IRI operation (IRI-1h, IRI-12h, IRI-24h, and IRI-48h, respectively). The respiratory rate, heart rate, and body temperature were monitored throughout the operation. All rabbits were successfully operated on.

MRI examination

All rabbits were scanned using a 3.0 T MRI system (750 w; GE Healthcare, Chicago, IL, USA) and a 16-channel phase array body coil. All rabbits were prevented from consuming food and water 8 hours before the MRI examination. The rabbits were anesthetized and placed on the scanning table in the left lateral decubitus position. During axial scanning, the positioning line was perpendicular to the long axis of the left kidney. The axial T2-weighted MRI parameters were as follows: repetition time (TR)/echo time (TE), 1,500/87 ms; slice thickness, 4 mm; gap, 1.0 mm; field of vision (FOV), 14 mm × 14 mm; matrix size, 256×224; flip angle, 111 degrees; bandwidth, 31.25 Hz per/pixel; and scan time, 1 min 52 s. QSM was acquired using a 3-dimensional (3D) multi-echo gradient echo (GRE) sequence with the following parameters: TR, 36.7 ms; TEs, 4.4 ms/9.2 ms/14.1 ms/18.9 ms/23.8 ms/28.6 ms; slice thickness, 2 mm; gap, 0 mm; FOV, 15 cm × 12 cm; matrix size, 448×176; flip angle, 10 degrees; and total scan time, 23 s.

MRI data analysis

All images were analyzed using STI Suite v. 3.0 (Medical Imaging, brain Imaging and Cell Modulation, University of California, Berkeley, CA, USA), a software package based on MATLAB R2016b (MathWorks, Natick, MA, USA) to postprocess the raw data of QSM. The image phase was first unwrapped using a Laplacian-based phase unwrapping algorithm. The background phase was removed with the complex harmonic artifact removal method. Streaking artifacts were reduced using the streaking artifacts reduction for QSM (STAR-QSM) algorithm. The axial renal hilum section was chosen for imaging analysis. The region of interest (ROI) was manually delineated along the margin of the outer medulla on the QSM image to calculate the magnetic susceptibility value (*Figure 1*). The axial T2-weighted image was used as a reference. Observer 1 (10 years of experience in abdominal radiology) and observer 2 (5 years of experience in abdominal radiology) drew the ROIs independently to test the interobserver reproducibility. Two observers were blinded to the histologic results.

Histologic analysis

At each time point, 6 rabbits from the IRI group were selected according to a random number table after the MRI examination. These rabbits were euthanized with an injection of 50 mL of air via the marginal ear vein under general anesthesia. All rabbits of the sham group were

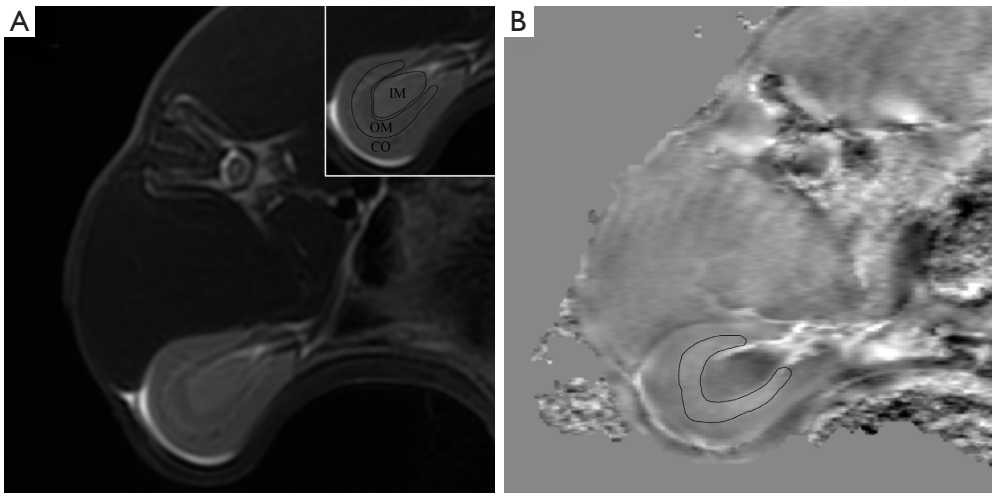

Figure 1 The diagram of the ROI. The ROI was manually delineated along the margin of the renal outer medulla on the QSM (B), and the axial T2-weighted images (A) were used as a reference. CO, cortex; IM, inner medulla; OM, outer medulla; ROI, region of interest; QSM, quantitative susceptibility mapping.

euthanized after the MRI examination at the IRI-48h time point. The left kidney was harvested for histopathological analysis. The transection of the kidney in the middle of the renal pedicle was divided into 2 parts, and 1 part was fixed with 10% neutral formalin solution. The axial renal hilum section was selected for hematoxylin and eosin (HE) and GPX4 immunohistochemistry. Tubular epithelial edema, tubular epithelial necrosis, interstitial inflammation, and cast were evaluated on the HE-stained images. Each histopathological feature was evaluated using a semiquantitative scoring scale in 5 random fields (×200 magnification) on each slice. Each histopathological feature was assessed using a semi-quantitative scoring scale: 0, none; 1, area <10%; 2, 10%≤ area <25%; 3, 25%≤ area <50%; 4, 50%≤ area <75%; 5, area ≥75%. The percentage represented the area of positive indicators in the whole FOV. The total score of pathological injury was the sum of each histopathological feature scores. The average optical density of GPX4 in 5 random fields (×200 magnification) on each slice was measured using ImageJ software (US National Institutes of Health, Bethesda, MD, USA). The results are expressed as the mean score in a single field. Another specimen was used to measure iron content.

The method for measuring the tissue iron content contained a number of steps. First, the tissue of the outer medulla was homogenized from the specimen in 9 volumes of normal saline using a homogenizer. Second, 0.5 mL of the supernatant was collected from the homogenate after using 10 min of centrifugation. Finally, the supernatant was used for the evaluation of iron content using a tissue iron determination kit (A039-2-1, Nanjing Jiancheng Bioengineering Institute, Nanjing, China).

The formula for calculating the iron content was as follows:

$$Iron\ content = \frac{OD_{sample} - OD_{control}}{OD_{standard} - OD_{control}} \times C_{standard} \div C_{sample} \quad [1]$$

where OD_{sample} is the sample optical density (OD) value, $OD_{control}$ is the control OD value, $OD_{standard}$ is the standard OD value, $C_{standard}$ is the standard concentration (35.81 μmol/L), and C_{sample} is the sample concentration (gprot/L).

Statistical analysis

SPSS 25.0 (IBM Corp, Armonk, NY, USA) was used for statistical analyses. The Shapiro-Wilk normality test was performed to check the normality of the data distribution. Quantitative data with normal distribution was presented as the mean ± standard deviation. The susceptibility values of the outer medulla in the sham group and the IRI group at different time points were compared using a repeated-measurement analysis of variance (ANOVA). One-way ANOVA was used to compare the differences in the average optical density value of GPX4. Differences in the pathological score of renal injury and iron content in the outer medulla were assessed using the nonparametric Kruskal-Wallis test. The intraclass correlation coefficient

(ICC) was used to compare the consistency between observers. Spearman correlation analysis was used to evaluate the correlation between the susceptibility values of the outer medulla and the pathological score of renal injury, the average optical density value of GPX4, and iron content in the outer medulla. A P value <0.05 was considered statistically significant.

Results

Interobserver consistency

The interobserver consistency (ICC =0.77; 95% CI: 0.619–0.864) was excellent for the susceptibility values.

The dynamic changes of the susceptibility values at different time points in the IRI group and the sham group

The susceptibility values of the outer medulla in the IRI group at the pre-IRI, IRI-1h, IRI-12h, IRI-24h, and IRI-48h time points were $(42.83\pm7.83)\times10^{-3}$, $(-5.33\pm6.28)\times10^{-3}$, $(6.50\pm3.94)\times10^{-3}$, $(12.00\pm3.74)\times10^{-3}$, and $(22.00\pm6.81)\times10^{-3}$ ppm, respectively. The susceptibility values of the outer medulla in the sham group at the pre-IRI, IRI-1h, IRI-12h, IRI-24h, and IRI-48h time points were $(40.83\pm8.77)\times10^{-3}$, $(42.33\pm10.67)\times10^{-3}$, $(40.00\pm6.10)\times10^{-3}$, $(39.17\pm6.34)\times10^{-3}$, and $(45.00\pm10.75)\times10^{-3}$ ppm, respectively. No significant differences were found in the susceptibility values of the outer medulla for the sham group among the different IRI time points (P>0.05). Statistical differences were found in the susceptibility values of the outer medulla at different time points in the IRI group (P<0.001). In the IRI group, there was no significant difference in susceptibility values of the outer medulla between the IRI-12h and IRI-24h time points. However, there were significant differences among the other time points.

At the IRI-1h, IRI-12h, IRI-24h, and IRI-48h time points, the susceptibility values in the sham group were all higher than those in the IRI group (all P values <0.05). In the IRI group, the susceptibility values of the outer medulla at the IRI-1h time point were the lowest, while the susceptibility values of the outer medulla at the IRI-12h, IRI-24h, and IRI-48h time points successively increased (*Figures 2,3*).

The pathological scores of renal injury, iron content in the outer medulla, and the average optical density of GPX4

Cell edema was most obvious at the IRI-1h time point and then decreased gradually. The scores of cell necrosis, interstitial inflammation, and cast increased gradually with the prolongation of reperfusion time (*Table 1*). The pathological score of renal injury was 0 in the IRI group at the pre-IRI time point and in the sham group. The iron content in the outer medulla at the IRI-1h time point was the lowest and then increased gradually. With the extension of reperfusion time, the average optical density of GPX4 decreased gradually (*Table 2*).

Correlation between the susceptibility values of the outer medulla and the histopathological scores, iron content, and the average optical density of GPX4

The susceptibility values of the outer medulla were negatively correlated with cell edema ($\rho=-0.61$; P=0.002) and the average optical density of GPX4 ($\rho=-0.70$; P<0.001). The susceptibility values of the outer medulla were positively correlated with iron content ($\rho=0.79$; P<0.001), the scores of cell necrosis ($\rho=0.71$; P<0.001), interstitial inflammation ($\rho=0.60$; P=0.002), cast ($\rho=0.75$; P<0.001), and the total pathological score of renal injury ($\rho=0.51$; P=0.01).

Discussion

The study investigated the dynamic relationship between the susceptibility values of the outer medulla and the pathological score of renal injury, iron content in the outer medulla, and the average optical density of GPX4. The results showed that the susceptibility values of the outer medulla were the lowest at the IRI-1h time point and increased gradually from the IRI-12h to IRI-48h time points. The susceptibility values of the outer medulla were negatively correlated with cell edema and the average optical density of GPX4 and positively correlated with other pathological scores of renal injury and iron content in the outer medulla.

This study mainly explored changes in the outer medulla during renal IRI. Two aspects may explain these findings. First, although the renal blood supply was abundant, the outer medulla only received about 10% of renal blood flow. It was susceptible to hypoxic injury (1). Second, the main structure of the outer medulla was the renal tubule, which required a large amount of oxygen consumption for reabsorption. The metabolism of the renal tubule was one of the determinants of the level of intrarenal oxygenation (17). Therefore, the outer medulla was prone to hypoxic injury (18,19). Previous studies have

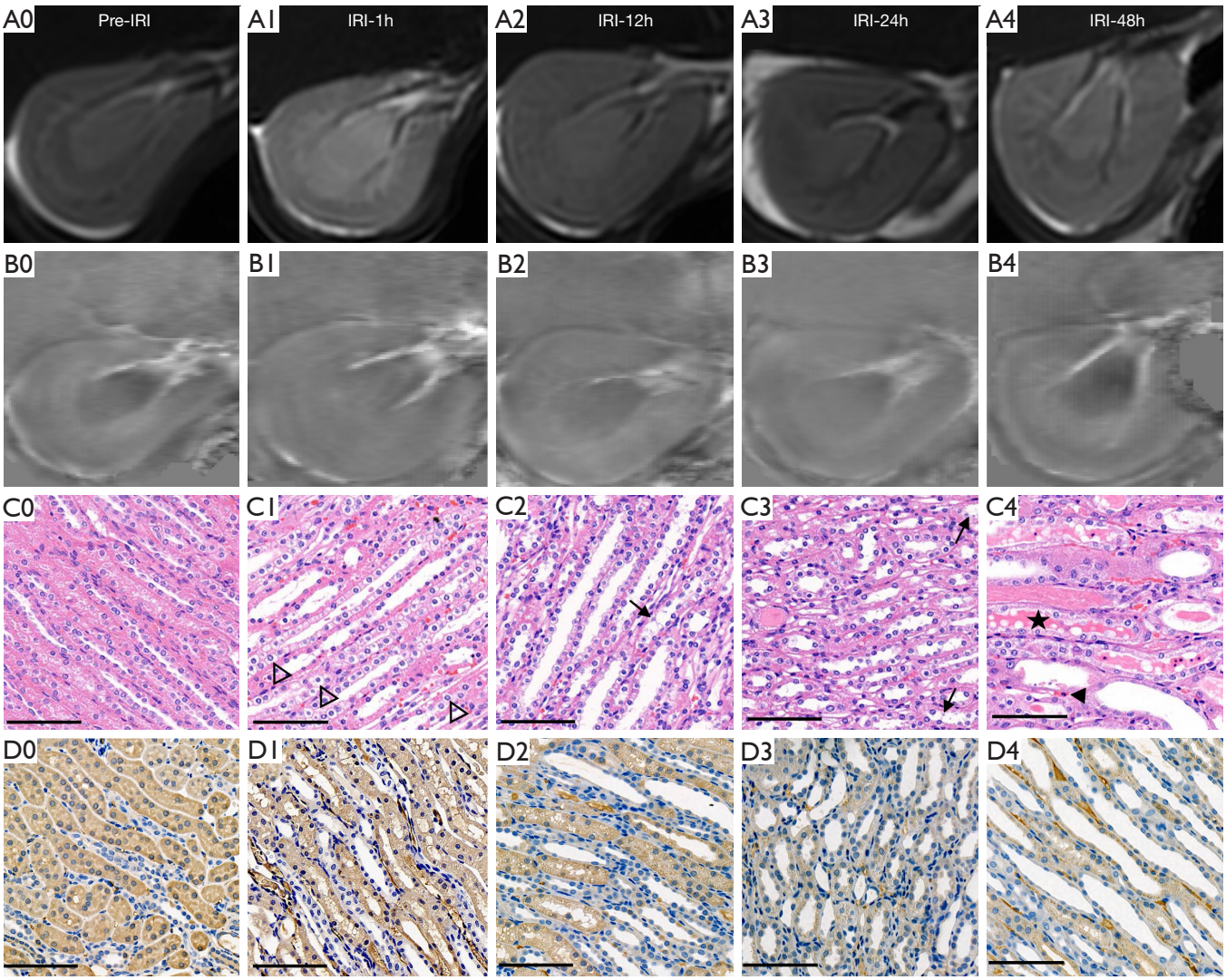

Figure 2 Representative MR images and pathology images at different time points in the IRI group. (A) T2-weighted images. (B) QSM images. The boundary of the inner medulla, outer medulla, and cortex was clear in the IRI group at the pre-IRI time point (A0, B0). The signal intensity of the outer medulla was lower at IRI-1h than at the pre-IRI time point (B1). The outer medulla zone widened slightly, and the boundary between the cortex and medulla was blurred in the IRI group at the IRI-1h time point (A1, B1). The signal intensity of the renal outer medulla gradually increased, and the boundary between cortex and medulla was clear at the IRI-12h, IRI-24h, and IRI-48h time points (A2–A4, B2–B4). (C) HE images (×400). In the IRI group at the pre-IRI time point (C0), the tubules were aligned. However, renal tubular epithelial cells showed marked swelling (△) at the IRI-1h time point (C1). At the IRI-12h and IRI-24h time points (C2, C3), parts of the brush edge of proximal convoluted tubules were destroyed, necrosis (↑) occurred in a few tubular epithelial cells. A part of the tubular lumen revealed dilatation, and red cell casts occurred. At the IRI-48h time point (C4), necrosis and casts (★) were aggravated, and there were inflammatory cells (▲) infiltrating into the renal interstitium. (D) GPX4 images (×400). In the IRI group at the pre-IRI time point (D0), the expression level of GPX4 was higher than that at the other time points. With the prolongation of reperfusion time, the expression level of GPX4 decreased gradually (D1–D4). Scale bar, 100 μm. MR, magnetic resonance; IRI, ischemia-reperfusion injury; QSM, quantitative susceptibility mapping; HE, hematoxylin and eosin; Pre-IRI, before the IRI operation; IRI-1h, 1h after the IRI operation; IRI-12h, 12h after the IRI operation; IRI-24h, 24h after the IRI operation; IRI-48h, 48h after the IRI operation; GPX4, glutathione peroxidase 4.

confirmed the main pathophysiological change of IRI to be the injury of renal tubular epithelial cells in the outer medulla (20). Ysebaert *et al.* (16) established a rat IRI model and found that about 80% of the proximal tubule cells in the outer medulla were damaged after 12 h of reperfusion. Liu *et al.* (21) also observed renal tubules and interstitial tissues of the outer medulla of the kidney damaged after renal IRI.

This study found that the susceptibility values of the outer medulla and the iron content of tissue were the lowest at the IRI-1h time point. Histopathological results demonstrated that at the IRI-1h time point, the tubular epithelial edema was the most obvious, but the average optical density of GPX4 was not significantly decreased. The susceptibility values of the outer medulla were negatively correlated with cell edema and the average optical density of GPX4. The results were consistent with those of previous studies (15,22). At the IRI-1h time point, the outer medulla was mainly characterized by cell edema. The swelling tubular epithelial cells compressed the capillary network, resulting in decreased blood flow (22). This study also showed no significant difference in susceptibility values between the IRI group at the pre-IRI time point and the sham group. Findings indicated that the procedure performed was gentle, with little or no bleeding from the muscles and perirenal tissue, which rarely affected the signal changes in the medulla of the kidney. Meanwhile, QSM provided good diagnostic images that differentiated the normal kidneys from other treated kidneys.

In addition, with the increase in the reperfusion time, the susceptibility values increased successively at the IRI-

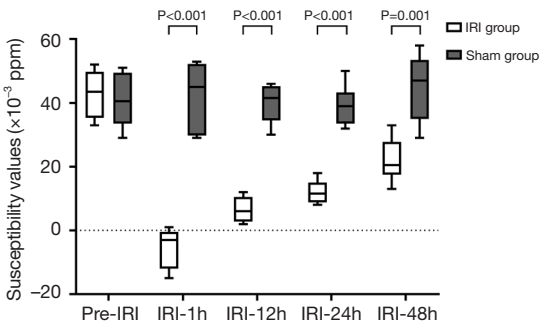

Figure 3 Dynamic changes of the susceptibility values of the outer medulla between the IRI group and the sham group at each time point. The susceptibility values of the IRI group and the sham group at the IRI-1h, IRI-12h, IRI-24h, and IRI-48h time points had statistically significant differences (all P values <0.05). IRI, ischemia-reperfusion injury; Pre-IRI, before the IRI operation; IRI-1h, 1h after the IRI operation; IRI-12h, 12h after the IRI operation; IRI-24h, 24h after the IRI operation; IRI-48h, 48h after the IRI operation.

Table 2 Iron content in the outer medulla and the average optical density of GPX4 in the IRI group

Time point	Iron content in the outer medulla (μmol/gprot)	The average optical density of GPX4
Pre-IRI (n=6)	6.57±1.49	0.23±0.04
IRI-1h (n=6)	3.03±0.41	0.20±0.01
IRI-12h (n=6)	3.41±0.55	0.20±0.02
IRI-24h (n=6)	4.22±0.99	0.13±0.03
IRI-48h (n=6)	6.01±1.51	0.11±0.02
F/H value	20.68	18.55
P value	<0.001	<0.001

Data are presented as mean ± standard deviation. GPX4, glutathione peroxidase 4; IRI, ischemia-reperfusion injury; Pre-IRI, before the IRI operation; IRI-1h, 1h after the IRI operation; IRI-12h, 12h after the IRI operation; IRI-24h, 24h after the IRI operation; IRI-48h, 48h after the IRI operation.

Table 1 Histopathological features of renal IRI in the IRI group at different time points

Histopathological Features	Pre-IRI (n=6)	IRI-1h (n=6)	IRI-12h (n=6)	IRI-24h (n=6)	IRI-48h (n=6)	H value	P value
Cell edema	0	3.83±1.20	2.67±1.03	2.00±0.63	1.67±0.52	11.14	<0.001
Cell necrosis	0	0.50±0.55	0.83±0.75	2.83±0.75	3.50±1.22	17.49	<0.001
Interstitial inflammation	0	1.33±0.52	2.33±0.82	2.50±0.55	3.33±1.03	12.02	<0.001
Cast	0	0.67±0.52	1.50±0.55	1.83±0.75	4.00±0.89	17.42	<0.001
Total score of pathological injury	0	6.67±1.86	7.33±2.50	9.17±2.14	12.50±3.39	10.08	<0.001

Data are presented as mean ± standard deviation. IRI, ischemia-reperfusion injury; Pre-IRI, before the IRI operation; IRI-1h, 1h after the IRI operation; IRI-12h, 12h after the IRI operation; IRI-24h, 24h after the IRI operation; IRI-48h, 48h after the IRI operation.

12h, IRI-24h, and IRI-48h time points. Meanwhile, histopathological results showed that cell necrosis, interstitial inflammation, and cast were gradually aggravated, and the average optical density of GPX4 gradually decreased during from 12 to 48 h after IRI. The iron content in the outer medulla increased gradually. The susceptibility values were positively correlated with iron content in the outer medulla, cell necrosis, interstitial inflammation, and cast. Zhang *et al.* (4) confirmed that, with the aggravation of renal IRI, the values of R2* (1/T2*) increase. This observation is consistent with that of our study. From 12 to 48 h after IRI, the expression of GPX4 decreased gradually, which suggests that ferroptosis increased gradually. The paramagnetic substance increased gradually with the increase of iron content in the tissue, which led to an increase in the susceptibility values of the outer medulla. Ding *et al.* (23) reported that ferroptosis occurred in renal tubular epithelial cells 48 h after IRI, and the intracellular free iron content was significantly higher than that before IRI.

This study had some limitations. First, the sample size was small. Second, QSM was susceptible to the artifacts derived from gastrointestinal gas and bleeding. However, during the MRI scanning, certain measures, such as fasting, were performed to reduce artifacts. Third, only renal IRI in the early stage was assessed with QSM, and thus the long-term effects of IRI will be explored in future studies. Fourth, there are many different pathophysiological mechanisms involved in the process of renal IRI, such as stagnant blood in the vasa recta (24). The next step of our study is to further investigate the interaction between different mechanisms in order to achieve a more comprehensive study of renal IRI. Finally, since this was an animal study, the results cannot be directly translated into clinical practice. However, more QSM application studies will provide additional scientific evidence (25,26). This study suggests that QSM may have clinical potential in evaluating human renal IRI.

Conclusions

The QSM technique could indirectly reflect the dynamic process of early renal IRI. The susceptibility values of the outer medulla showed a good correlation with the pathological score of renal injury, indicating the susceptibility values could reflect the pathological injury during the IRI process. The iron content in the outer medulla and the average optical density of GPX4 significantly differed across the different time points. Furthermore, the susceptibility values had a good correlation with iron content in the outer medulla and the average optical density of GPX4, suggesting that the susceptibility values could reflect changes in ferroptosis in renal IRI. In general, QSM is a feasible, noninvasive tool for imaging and evaluating changes in renal IRI.

Acknowledgments

Funding: This study was funded by the National Natural Science Foundation Project of China (Nos. 81901696 and 81971572) and Top Talent of Changzhou "The 14th Five-Year Plan" High-Level Health Talents Training Project (No. 2022260).

Footnote

Reporting Checklist: The authors have completed the ARRIVE reporting checklist. Available at https://qims.amegroups.com/article/view/10.21037/qims-22-838/rc

Conflicts of Interest: All authors have completed the ICMJE uniform disclosure form (available at https://qims.amegroups.com/article/view/10.21037/qims-22-838/coif). WD is an employee of GE Healthcare in China. The other authors have no conflicts of interest to declare.

Ethical Statement: The authors are accountable for all aspects of the work in ensuring that questions related to the accuracy or integrity of any part of the work are appropriately investigated and resolved. Experiments were performed under a project license (No. 2020-120) granted by the institutional ethics board of The Third Affiliated Hospital of Soochow University in compliance with institutional guidelines for the care and use of animals.

References

1. Munshi R, Hsu C, Himmelfarb J. Advances in

understanding ischemic acute kidney injury. BMC Med 2011;9:11.
2. Basile DP, Anderson MD, Sutton TA. Pathophysiology of acute kidney injury. Compr Physiol 2012;2:1303-53.
3. Hueper K, Rong S, Gutberlet M, Hartung D, Mengel M, Lu X, Haller H, Wacker F, Meier M, Gueler F. T2 relaxation time and apparent diffusion coefficient for noninvasive assessment of renal pathology after acute kidney injury in mice: comparison with histopathology. Invest Radiol 2013;48:834-42.
4. Zhang B, Wang Y, Wang C, Wang H, Kong H, Zhang J, Zou Y, Yang M. Comparison of blood oxygen level-dependent imaging and diffusion-weighted imaging in early diagnosis of acute kidney injury in animal models. J Magn Reson Imaging 2019;50:719-24.
5. Park SY, Kim CK, Park BK, Kim SJ, Lee S, Huh W. Assessment of early renal allograft dysfunction with blood oxygenation level-dependent MRI and diffusion-weighted imaging. Eur J Radiol 2014;83:2114-21.
6. Pohlmann A, Arakelyan K, Seeliger E, Niendorf T. Magnetic Resonance Imaging (MRI) Analysis of Ischemia/Reperfusion in Experimental Acute Renal Injury. Methods Mol Biol 2016;1397:113-27.
7. Hueper K, Gutberlet M, Rong S, Hartung D, Mengel M, Lu X, Haller H, Wacker F, Meier M, Gueler F. Acute kidney injury: arterial spin labeling to monitor renal perfusion impairment in mice-comparison with histopathologic results and renal function. Radiology 2014;270:117-24.
8. Liu C, Li W, Tong KA, Yeom KW, Kuzminski S. Susceptibility-weighted imaging and quantitative susceptibility mapping in the brain. J Magn Reson Imaging 2015;42:23-41.
9. Wang Y, Liu T. Quantitative susceptibility mapping (QSM): Decoding MRI data for a tissue magnetic biomarker. Magn Reson Med 2015;73:82-101.
10. Wang F, Zhang M, Li Y, Li Y, Gong H, Li J, Zhang Y, Zhang C, Yan F, Sun B, He N, Wei H. Alterations in brain iron deposition with progression of late-life depression measured by magnetic resonance imaging (MRI)-based quantitative susceptibility mapping. Quant Imaging Med Surg 2022;12:3873-88.
11. Deistung A, Schweser F, Reichenbach JR. Overview of quantitative susceptibility mapping. NMR Biomed 2017. doi: 10.1002/nbm.3569.
12. Yamada N, Karasawa T, Wakiya T, Sadatomo A, Ito H, Kamata R, Watanabe S, Komada T, Kimura H, Sanada Y, Sakuma Y, Mizuta K, Ohno N, Sata N, Takahashi M. Iron overload as a risk factor for hepatic ischemia-reperfusion injury in liver transplantation: Potential role of ferroptosis. Am J Transplant 2020;20:1606-18.
13. Su L, Jiang X, Yang C, Zhang J, Chen B, Li Y, Yao S, Xie Q, Gomez H, Murugan R, Peng Z. Pannexin 1 mediates ferroptosis that contributes to renal ischemia/reperfusion injury. J Biol Chem 2019;294:19395-404.
14. Linkermann A, Skouta R, Himmerkus N, Mulay SR, Dewitz C, De Zen F, et al. Synchronized renal tubular cell death involves ferroptosis. Proc Natl Acad Sci U S A 2014;111:16836-41.
15. Chen J, Chen Q, Zhang J, Pan L, Zha T, Zhang Y, Chen J. Value of T2 Mapping in the Dynamic Evaluation of Renal Ischemia-Reperfusion Injury. Acad Radiol 2022;29:376-81.
16. Ysebaert DK, De Greef KE, Vercauteren SR, Ghielli M, Verpooten GA, Eyskens EJ, De Broe ME. Identification and kinetics of leukocytes after severe ischaemia/reperfusion renal injury. Nephrol Dial Transplant 2000;15:1562-74.
17. Hueper K, Peperhove M, Rong S, Gerstenberg J, Mengel M, Meier M, Gutberlet M, Tewes S, Barrmeyer A, Chen R, Haller H, Wacker F, Hartung D, Gueler F. T1-mapping for assessment of ischemia-induced acute kidney injury and prediction of chronic kidney disease in mice. Eur Radiol 2014;24:2252-60.
18. Bonventre JV, Yang L. Cellular pathophysiology of ischemic acute kidney injury. J Clin Invest 2011;121:4210-21.
19. Haase VH. Mechanisms of hypoxia responses in renal tissue. J Am Soc Nephrol 2013;24:537-41.
20. Havasi A, Borkan SC. Apoptosis and acute kidney injury. Kidney Int 2011;80:29-40.
21. Liu X, Murphy MP, Xing W, Wu H, Zhang R, Sun H. Mitochondria-targeted antioxidant MitoQ reduced renal damage caused by ischemia-reperfusion injury in rodent kidneys: Longitudinal observations of T(2) -weighted imaging and dynamic contrast-enhanced MRI. Magn Reson Med 2018;79:1559-67.
22. Pohlmann A, Hentschel J, Fechner M, Hoff U, Bubalo G, Arakelyan K, Cantow K, Seeliger E, Flemming B, Waiczies H, Waiczies S, Schunck WH, Dragun D, Niendorf T. High temporal resolution parametric MRI monitoring of the initial ischemia/reperfusion phase in experimental acute kidney injury. PLoS One 2013;8:e57411.
23. Ding C, Ding X, Zheng J, Wang B, Li Y, Xiang H, Dou M, Qiao Y, Tian P, Xue W. miR-182-5p and miR-378a-3p regulate ferroptosis in I/R-induced renal injury. Cell Death Dis 2020;11:929.

24. Taylor A, Sharkey J, Harwood R, Scarfe L, Barrow M, Rosseinsky MJ, Adams DJ, Wilm B, Murray P. Multimodal Imaging Techniques Show Differences in Homing Capacity Between Mesenchymal Stromal Cells and Macrophages in Mouse Renal Injury Models. Mol Imaging Biol 2020;22:904-13.
25. Qu Z, Yang S, Xing F, Tong R, Yang C, Guo R, Huang J, Lu F, Fu C, Yan X, Hectors S, Gillen K, Wang Y, Liu C, Zhan S, Li J. Magnetic resonance quantitative susceptibility mapping in the evaluation of hepatic fibrosis in chronic liver disease: a feasibility study. Quant Imaging Med Surg 2021;11:1170-83.
26. Bechler E, Stabinska J, Thiel T, Jasse J, Zukovs R, Valentin B, Wittsack HJ, Ljimani A. Feasibility of quantitative susceptibility mapping (QSM) of the human kidney. MAGMA 2021;34:389-97.

Cite this article as: Luo K, Yu A, Fu Q, Pan L, Dou W, Zhang J, Chen J. Renal ischemia-reperfusion injury in rabbits evaluated with quantitative susceptibility mapping: an animal study. Quant Imaging Med Surg 2023;13(4):2441-2450. doi: 10.21037/qims-22-838

